DiffPhysiNet: A Bearing Diagnostic Framework Based on Physics-Driven Diffusion Network for Unseen Working Conditions

Zhibin Guo[1] Jingsong Xie[2] Tongyang Pan[3] and Tiantian Wang[4]

[1,2,3,4] *School of Traffic & Transportation Engineering, Central South University, China*

marcogzb@csu.edu.cn
jingsongxie@foxmail.com
ty.pan@csu.edu.cn
wangtt@hnu.edu.cn

ABSTRACT

Fault diagnosis is essential to ensure bearing safety in industrial applications. Many existing diagnostic methods require large scales of data from a full range of working conditions. However, the structure and working conditions differences between machines lead to significant variation in data distribution, making it difficult to diagnostic with unseen samples. To handle this situation, an unknown condition diagnosis Framework (UCDF) based on physics-driven diffusion network (DiffPhysiNet) is proposed, effectively integrating the generation capability of the diffusion model and learning from the working conditional encoding (WCE). Specifically, signals under limited working conditions are gradually convert to noise through a forward noising process. Then, DiffPhysiNet reconstructs signals from the noise by a reverse denoising process. In addition, a physics-driven UNet (Physi-UNet) structure is designed to extract WCE for noise level prediction during the reverse process. Moreover, an Unsupervised Clustering Filter (UCFilter) is constructed to select signals with high quality after generation. Signals under unknown working condition can be generated with certain WCE. Ultimately, extensive experiments on two bearing datasets (SDUST and PU) validate the effectiveness of our method compared with the state-of-the-art baselines and the ablution test confirms the significant role of Physi-UNet and UCFilter.

1. INTRODUCTION

Rotating machinery is crucial in modern industry, highlighting the need for effective condition monitoring and fault diagnosis technology to ensure its security and reliability (Kordestani et al. 2021). Deep learning-based approaches have gained significant attention in machine condition monitoring as a data-driven fault diagnosis method(Zio 2022).

For deep learning to effectively diagnose faults in rotating machinery, it requires consistency in the data distribution between training and testing sets. However, practical industrial applications often present challenges that hinder the applicability of deep learning methods, which can be concluded as follows: **(1)** Rotating components often operate under varied conditions, such as changes in rotational speed and load (Chen and Li 2017). **(2)** Obtaining sufficient labeled data with precise health information across all operating conditions can be impractical. **(3)** Domain shift issues arise when attempting to compensate for information gaps by utilizing labeled data from multiple machines or different working conditions. Also, due to discrepancies in data (Ben-David et al. 2010).

In recent years, various advanced techniques have been developed to tackle the aforementioned challenges. One of these techniques is domain adaptation (DA), which aims to reduce the distribution discrepancy between the source and target domains during model training (Wang et al. 2020). DA allows the transfer of knowledge acquired from large source datasets to construct diagnostic models for smaller target datasets with similar characteristics. Wang et al. proposed the use of intra-class maximum mean discrepancy (MMD) in conjunction with multi-scale ResNet architectures to reduce the conditional distribution discrepancy of vibration signals (Wang et al. 2020). Hu et al. introduced tensor-aligned invariant subspace learning, which enables the discovery of a shared tensor representation for cross-domain diagnosis cases (Hu, Wang, and Gu 2020). Inspired by adversarial learning principles, Li et al. developed a method to map knowledge from target to source working conditions using generative adversarial networks (Li et al. 2021). Domain adaptation techniques can improve the robustness and generalization capabilities of fault diagnosis models. However, these methods are limited by the closed-set assumption, meaning that the source and

target domains have feature distributions that cannot be crossed (Si et al. 2021).

Under this premise, it is necessary to develop a technique that takes the out-of-distributed (OOD) fault classification into account (Michau and Fink 2019). Generative Adversarial Networks (GANs) nowadays adopts an unsupervised learning method and automatically learns from the source data. In the applications of PHM, conditional GANs have been used to control the generation process to generate desired distinct classes. Wang et al. introduced an enhanced version of Least-Square Generative Adversarial Networks (LSGANs) which notably retain more signal details compared to traditional methods and exhibit significant robustness (Wang et al. 2019). However, these methods are only suitable for generating data from previously observed conditions and not for generating previously unseen conditions in a specific domain (Rombach, Michau, and Fink 2023). The latter is the focus of our research. For the issue of the diagnostic works under unseen working conditions, propose a new framework for Open-Partial DA based on generating distinct fault signatures with a Wasserstein GAN, which enables a better transferability between two different domains (Li et al. 2022). However, the main drawback of GANs is that they are unstable during the training process and it is hard to embed diagnostic knowledge during the process of generation(Cui et al. 2023). Nowadays, same as a generative model, diffusion model does not suffer from GANs-like problems of training non-convergence and pattern collapse.

To achieve the stable and effective diagnostic framework for unseen working conditions based on feature embedding, we first propose a Physics-Driven Diffusion Network (DiffPhysiNet) for unknown condition diagnosis, which can generate a complete bearing sample of industrial environments and maintain the real-world working conditions through physics-informed methods. DiffPhysiNet effectively integrates the generation capability of the diffusion model and embeds working conditional encoding (WCE). Essentially, the forged signals generated by DiffPhysiNet guarantee the generation accuracy while retaining the utility. To summarize, the primary contributions of this work are concluded as follows:

- A denoising diffusion-based generative model DiffPhysiNet is proposed, which can generate high-quality signal data.
- A novel neural network structure called Physi-UNet, which integrates the residual block and attention mechanism to model signal features of bearings.
- UCFilter is constructed based on K-means clustering method to select the valuable signals after generation.

The remainder of the paper is structured as follows: In Section 2, we provide background information relevant to our research and in Section 3, we formally introduce the proposed diagnostic framework and its components in detail. Section 4 outlines the dataset utilized and presents the experimental results and in Section 6, we summary our work and proposes some research directions for the future.

2. PRELIMINARY

In this section, we first briefly introduce the basic knowledge of Denoising Diffusion Probabilistic Models (DDPM) (Shu, Li, and Farimani 2023) and Fourier Neural Operator (FNO)(Rafiq, Rafiq, and Choi 2022), which are the fundamentals of the proposed DiffPhyisNet.

2.1. Diffusion model

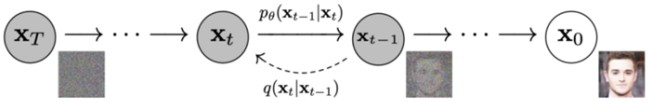

Figure 1. Two processes in Denoising Diffusion Probabilistic Models

As shown in Figure **1**, the diffusion model that typically contains two processes: forward process and reverse process. In this setting, a sample from the data distribution $x_0 \sim q(x)$ is gradually noised into a standard Gaussian noise $x_T \sim \mathcal{N}(0, I)$ by the forward process, where the transition is parameterized by $q(x_t \mid x_{t-1}) = \mathcal{N}\left(x_t; \sqrt{1-\beta_t}x_{t-1}, \beta_t \mathbf{I}\right)$ with $\beta_t \in (0,1)$ as the amount of noise added at diffusion step t.

A neural network learns the reverse process of gradually denoising the sample via reverse transition $p_\theta(x_{t-1}|x_t) = \mathcal{N}(x_{t-1};\, \mu_\theta(x_t,t), \sum \theta(x_t,t))$ .Learning to clean x_T through the reversed diffusion process can be reduced to learning to build a surrogate approximator to parameterize $\mu_\theta(x_t,t)$ for all t. The denoising model $\mu_\theta(x_t,t)$ can be trained by using a weighted mean squared error loss which we will refer to as:

$$\mathcal{L}(x_0) = \sum_{t=1}^{T} \mathop{\mathbb{E}}_{q(x_t|x_0)} \|\mu(x_t,x_0) - \mu_\theta(x_t,t)\|^2 \qquad (1)$$

where $\mu(x_t,x_0)$ is the mean of the posterior $q(x_t \mid x_{t-1})$. This objective can be justified as optimizing a weighted variational lower bound on the data log likelihood. Also note that the original parameterization of $\mu_\theta(x_t,t)$ can be modified in favor of $\hat{x}_0(x_t,t,\theta)$or$\epsilon_\theta(x_t,t)$.

2.2. Fourier neural operator

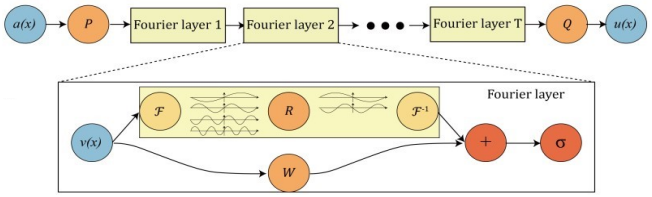

Figure 2. The full architecture of neural operator

The main idea of FNO is to use Fourier transform to map high-dimensional data into the frequency domain and approximate nonlinear operators by learning the relationships between Fourier coefficients through neural networks. The FNO architecture is shown in **Figure 2**, which consists of three main steps:

a) The input $a(x)$ is lifted to a higher dimensional representation $v_0(x) = P\big(a(x)\big)$ by the local transformation P, which is commonly parameterized by a shallow fully connected neural network.

b) The higher dimensional representation $v_0(x)$ is updated iteratively by:

$$v_{t+1}(x) = \sigma\big(W v_t(x) + (\mathcal{K}(a;\phi)v_t)(x)\big) \qquad (2)$$

where $(\mathcal{K}(a;\phi)v_t)(x)$ is a linear transform on the frequency domain of the amplitude and the phase of $v_t(x)$, W: is a linear transform on the high-dimension of the time domain. σ: is the non-linear activation function.

c) The output $u(x)$ is obtained by $u(x) = Q\big(v_T(x)\big)$, where Q : is the projection of v_T , and it is parameterized by a fully connected layer.

$\mathcal{F}$ and $\mathcal{F}^{-1}$are denoted as Fourier transform and its inverse transform of a function, allowing the operations on the frequency domain of the high-dimension. The Fourier neural operator (FNO)(Lehmann et al. 2024) aims to map between two infinite-dimensional spaces by training on a finite set of input–output pairs. It has been demonstrated that the FNO can serve as a universal approximator capable of accurately representing any continuous operator.

3. PROPOSED METHOD

In this section, we elaborate on the proposed DiffPhysiNet framework as shown in Figure 3. We start by presenting the diagnostic principles and steps of the proposed method under unseen working conditions. Then, we introduce the details of the denoising model, i.e., Physi-UNet. Furthermore, UCFiler utilize K-means to cluster some generated sample to prove the generation quality is also introduced.

3.1. Diagnostic principles of DiffPhysiNet

As illustrated in **Figure 3**, aiming at the diagnostic under unseen working conditions, 4 parts (a-d) are involved in the framework.

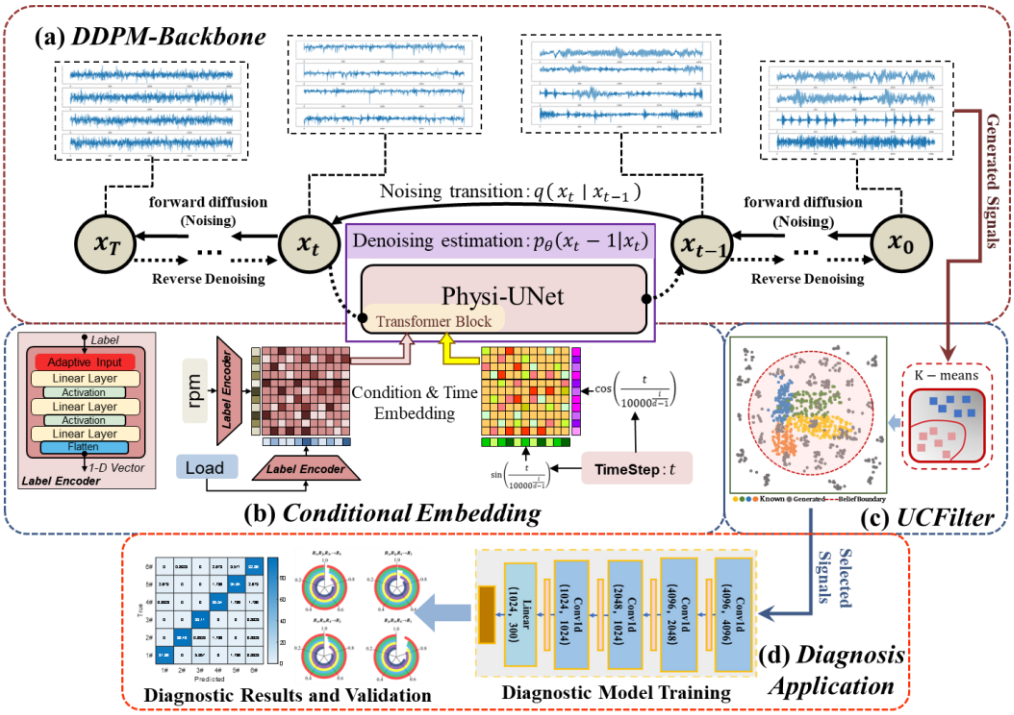

Figure 3. The diagram of proposed DiffPhysiNet framework

(a) The first part is based on the diffusion model which is introduced in **2.1**, utilizing this generative model rather than other generative methods mainly attribute to the style embedding convenience which ensures that generated fault signatures contain physics-driven features. (b) The second part aims to construct a latent space with conditional

encoding methods, making sure of that the projection space of working conditions are continuous. (c) The third part utilizes an unsupervised clustering method to select qualified generated signals guaranteeing the effectiveness of the training datasets. (d) The last part is the application stage of this proposed method, utilizing the selection of generated signals for the diagnostic model training. Then the validated diagnostic model can be applied for online fault diagnosis.

3.2. Structure of Physi-UNet

As aforementioned, the diffusion model (DDPM), A neural network learns the reverse process of gradually denoising the sample via reverse transition $p_\theta(x_{t-1}|x_t) = \mathcal{N}(x_{t-1};\ \mu_\theta(x_t,t), \sum\theta(x_t,t))$ .Learning to clean x_T through the reversed diffusion process can be reduced to learning to build a surrogate approximator to parameterize $\mu_\theta(x_t,t)$ for all t. In our proposed framework, Physi-UNet is utilized for the process of denoising estimation, of which the structure is shown in **Figure 4**. As illustrated in the figure, an implicit U-Net is introduced to enhance Fourier neural operator. The denoised signal after $(T-t)$ steps is utilized as the input, which is then converted into a high-dimensional representation via the lifting layer P, and finally the output is obtained through the projection of Q, converting the vectors from a high-dimensional space to 1D vibration signal (Benitez et al. 2023) .

The structural design of the Physi-UNet is based on the hypothesis that the Fourier spectrum of fault data can be expressed as the sum of (1) domain-specific components (the spectrum of a signal from normal operation) and (2) of fault-specific components representing the specific fault characteristics. In other words, this hypothesis allows us to express Fourier coefficients (Dang and Ishii 2022) of the fault data of a certain class c from a specific domain $\mathbb{X}$ ($x_{fault,\mathbb{X}}^{c,FFT}$) as a sum of domain-specific characteristics that are represented by the domain features $x_{\mathbb{S}}^{FFT}$ and the fault class specific characteristics that are domain-independent $x_{fault}^{c,FFT}$ $fault$ and scaled by a factor w, which can be expressed by:

$$x_{fault,\mathbb{X}}^{c,FFT} = x_{\mathbb{X}}^{FFT} + w * x_{fault}^{c,FFT} \tag{3}$$

The physics-driven fault component and the domain specific features are demodulated based on the embedding of Times Step t and the continuous working conditional encoding (WCE), which is of great importance on the guidance of feature decomposition. As shown in **Eq. (4)**.

$$\begin{cases} Attention(Q,K,V) = softma\,\boldsymbol{x_t}\left(\dfrac{QK^\top}{\sqrt{d}}\right)\cdot V \\ x_{fault,\mathbb{X}}^{c,FFT} = \boldsymbol{x_t} + Attention(Q,K,V) \\ Q = W_Q\cdot x_t, K = W_K\cdot x_t, V = W_V\cdot x_t \end{cases} \tag{4}$$

where $\boldsymbol{x_t} \in \mathbb{R}^{c\times n}$ (c and n represent the dimensions and length of the signal) is the given input, W_Q, W_K, and W_V are learnable parameter matrices from the embedded Timestep t and the encoded working condition.

Hence, the fault components of the vibration signals are captured in using Fourier bases:

$$A_{i,t}^{(k)} = \left|\mathcal{F}(x_{fault,\mathbb{X}}^{c,FFT})_k\right|, \Phi_{i,t}^{(k)} = \phi\left(\mathcal{F}(x_{fault,\mathbb{X}}^{c,FFT})_k\right), \tag{5}$$

$$\kappa_{i,t}{}^{(1)},\cdots,\kappa_{i,t}^{(K)} = \underset{k\in\left\{1,\cdots,\left\lfloor\frac{\tau}{2}\right\rfloor+1\right\}}{arg\,TopK}\left\{A_{i,t}^{(k)}\right\}, \tag{6}$$

$$P_{i,t}(x) = \sum_{k=1}^{K} A_{i,t}^{\kappa_{i,t}^{(k)}}\ cos\left(2\pi f_{\kappa_{i,t}^{(k)}}\tau c + \Phi_{i,t}^{\kappa_{i,t}^{(k)}}\right), \tag{7}$$

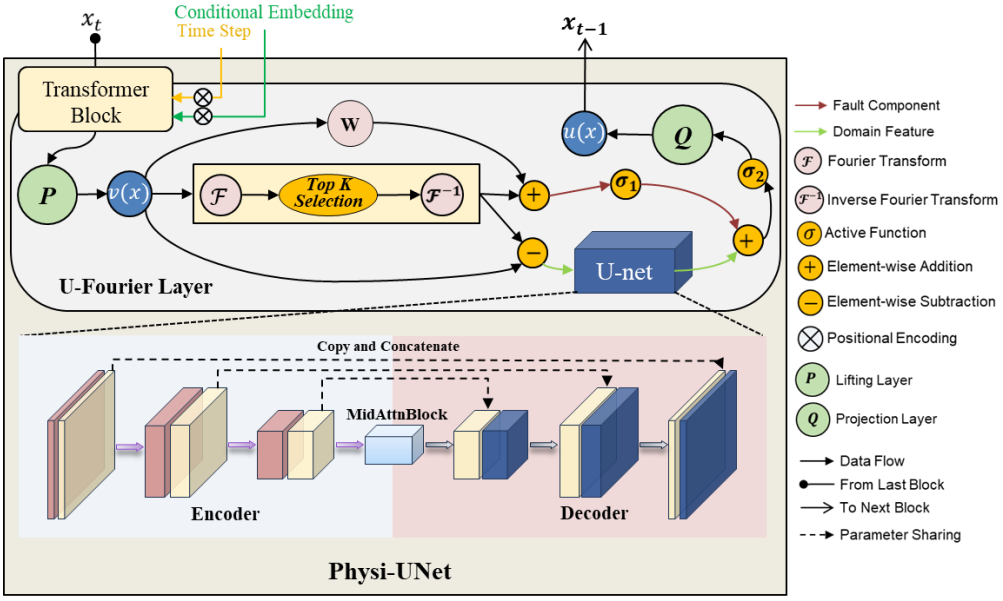

Figure 4. The structure of proposed Physi-UNet enhanced with FNO and U-Net component

where arg TopK is to get the top K amplitudes and K is a hyperparameter. $A_{i,t}^{(k)}$, $\Phi_{i,t}^{(k)}$ are the phase, amplitude of the k-th frequency after the discrete Fourier transform $\mathcal{F}$ respectively. f_k represents the Fourier frequency of the corresponding index k. In fact, the Fourier layer selects bases with the most significant amplitudes in the frequency domain, and then returns to the time domain through an inverse transform to model the physics-driven fault features.

The U-Net structure is utilized to synthesis the corresponding domain features according to the residue component after removing the fault frequencies.

$$D_{i,t}(x) = UNet(v_0(x) - P_{i,t}(x)) \tag{8}$$

where the $P_{i,t}$ is selected fault component and the $D_{i,t}$ is the obtained domain features.

$D_{i,t}$ and $P_{i,t}$ are then reweighted and activated in the following process, the summation and projection combine the physic-driven and domain feature components, which can be expressed as:

$$C_{i,t}(x) = \sigma_2\left[UNet(v_0(x) - P_{i,t}) + \sigma_1[W(P_{i,t})]\right] \tag{9}$$

$$x_{t-1} = Q\left(C_{i,t}(x)\right) \tag{10}$$

where $\sigma_1[\cdot]$ and $\sigma_2[\cdot]$ are the activation function, $W(\cdot)$is the reweight layer, $Q(\cdot)$ is the projection layer aforementioned, $x_{t-1}$is the out put of this diffusion step.

3.3. Unsupervised Clustering Filter

Once the DDPM in the DiffPhysiNet training is completed, the working conditions of signal generation is controlled by the WCE. As shown in Figure **5**. the generated signal clustered by K-means algorithm, which is an unsupervised clustering method. The top of n samples nearest to the signal sample center selected as valuable signals.

The distances between inter-class samples are measured by distribution probability based on Kullback-Leibler divergence between the joint probabilities R_{ij} in the high-dimensional space and the joint probabilities T_{ij} in the low-dimensional space. The values of R_{ij} are defined to be the symmetrized conditional probabilities, whereas the values of T_{ij} are obtained by means of the Student’ s t-distribution with one degree of freedom. The calculation is summarized as follows:

$$r_{ij} = \frac{r_{i|j} + r_{j|i}}{2n} \tag{11}$$

$$t_{ij} = \frac{\left(1 + |y_i - y_j|^2\right)^{-1}}{\sum_{k \neq l}(1 + |y_k - y_l|^2)^{-1}} \tag{12}$$

where $r_{i|j}$ is the distribution probability of sample point j when the sample point i is given. y is the generated samples. The values of r_{ii} and t_{ii} are set to zero. The calculation of the Kullback–Leibler divergence C_d between the two joint probability distributions R and T is given as follows:

$$C_d = KL(R\,||T) = \sum_i \sum_j r_{ij} \log r_{ij} - r_{ij} \log t_{ij} \tag{12}$$

After calculated the Kullback–Leibler divergence C_d of every sample in generated signals, the selection boundaries are decided according to the expectation numbers of acceptable samples n, and k value of the ***Boundary Decision*** indicates the portion of selected samples (k=n/N).

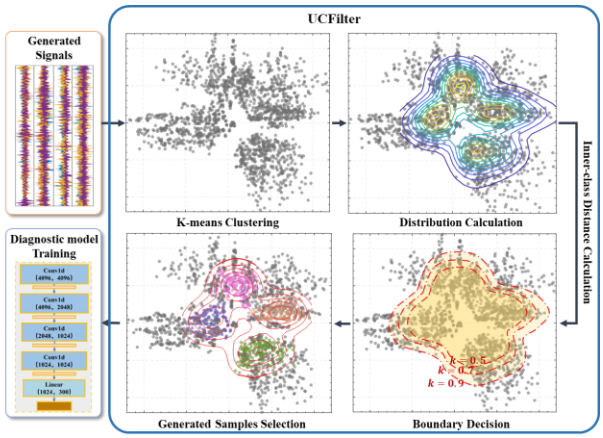

Figure 5. The steps of unsupervised clustering filter method

4. Experimental Validation

4.1. Experiments Setting

To assess the diagnostic model's performance in unfamiliar conditions, we conducted two experimental case studies using test rigs from SDUST (Jia et al. 2020) and the Paderborn University bearing dataset (PU dataset) for bearing fault diagnosis. The first case involves a constant domain shift with the rig operating at various constant speeds, while the second case examines a constant domain shift with the rig operating under multiple conditions of variable rotational speeds and loads. These experiments confirm the effectiveness of the DiffPhysiNet method, which utilizes diffusion models, for complex industrial applications.

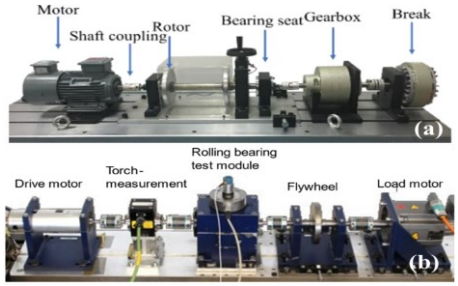

Figure 6. Experimental platform of SDUST dataset (a) and PU dataset (b).

4.1.1. Description of SDUST dataset and Case1

Figure **6** (a) shows the experimental platform of SDUST, which includes a motor, a shaft coupling, a rotor, a testing bearing, a gearbox, and a break.The bearing type utilized is N205EU, with data collected across four health conditions: normal (NOR), inner ring fault (I), rolling element fault (B), and outer ring fault (O). Four distinct working conditions were tested at speeds of 1000, 1500, 2000, and 2500r/min. The experiment sets four diagnostic cases for unseen working conditions across domains: T1000, T1500, T2000, and T2500 as shown in Table 1.

Table 1. **Case1:** Diagnostic cases of SDUST dataset.

Diagnostic cases	Seen Domain	Unseen Domain
T1	1500r/min,2000r/min,2500r/min	1000r/min
T2	1000r/min,2000r/min,2500r/min	1500r/min
T3	1000r/min,1500r/min,2500r/min	2000r/min
T4	1000r/min,1500r/min,2000r/min	2500r/min

4.1.2. Description of PU dataset and Case2

The test rig of PU dataset is shown in Figure **6** (b), which is mainly composed of a motor, a torque measurement shaft, a bearing test module, a flywheel, and a load motor. There are 7 health conditions, normal (N), inner-race fault (IF) with three damage levels (IF1, IF2, and IF3), outer-race fault (OF) with two damage levels (OF1 and OF2), and compound fault (CF) containing IF and OF.

Faulty bearings with real damage were acquired from an accelerated lifetime test. Vibration data was collected under four distinct working conditions, involving rotational frequency (Hz), load torque (Nm), and radial force (N), at a sampling frequency of 64 kHz. These conditions create four domains: P1, P2, P3, and P4, leading to four diagnosis cases, as outlined in Table 2. Each category in unseen working conditions comprises 2000 samples.

Table 2. **Case2:** Diagnostic cases of PU dataset.

Domain	Rotational frequency	Load	Diagnostic Cases	Seen Domain	Unseen Domain
p1	25Hz	1000N	**R1**	*p2, p3, p4*	*p1*
p2	15Hz	400N	**R2**	*p1, p3, p4*	*p2*
p3	15Hz	1000N	**R3**	*p1, p2, p4*	*p3*
p4	25Hz	400N	**R4**	*p1, p2, p3*	*p4*

4.1.3. Compared methods

Some typical or up-to-date technologies were utilized as a set of compared methods to validated the effectiveness of the DiffPhysiNet framework with the idea of Physi-UNet and UCFilter and all the methods used the same preprocessing and network back-bone for a fair comparison. As shown in Table 3, M1-M6 series are competitive related methods, M1 means the Domain Adaption (DA) method based on empirical risk minimization (ERM) principle using multi-domain data based on the general cross-entropy loss of DA method. M2-M4 follow the same setting in (Jiao et al. 2020; Huang et al. 2022; Han, Li, and Qian 2021) by adding a distance metric or distribution alignment as a loss term, such as MMD, JMMD, and CORAL. M5 (Li et al. 2020) is a start-of-the-art method DG that uses adversarial training with normalization strategies and a strategy of multi-case training and M6 (Chen et al. 2022) is a competitive method for cross-domain diagnosis under unseen domain through triplet loss and data augmentation with Gaussian noise.

Table 3. Related methods for comparation

Methods	Description
M1	DA
M2	DA with MMD
M3	DA with JMMD
M4	DA with CORAL
M5	ADIG (Li et al. 2020)
M6	IEDGNet (Chen et al. 2022)

4.2. Experimental results and analysis

4.2.1. Generated signal and analysis

To assess the effectiveness of the proposed diagnostic framework, we illustrate the generated signals in Figure **7**. Notably, there were no fault samples with a 1000N load and an rpm of 40Hz in the training set, yet similar fault samples were generated. Thus, DiffPhysiNet can generate fault signals for unseen combinations of rpm and load.

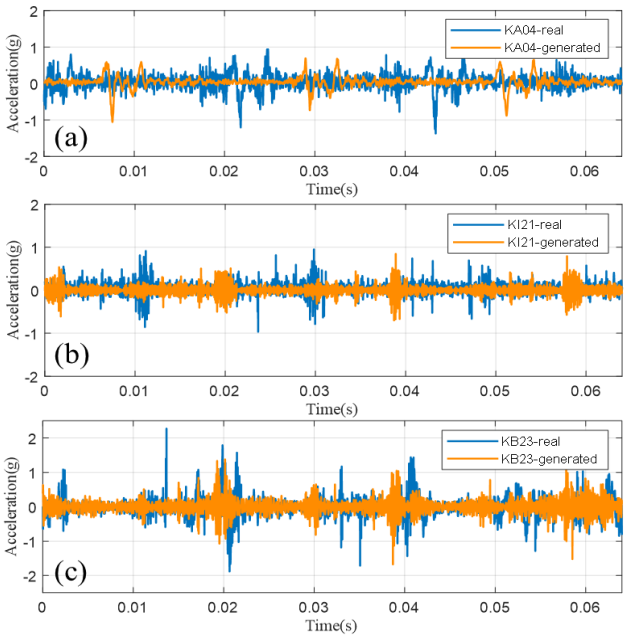

Figure 7. Generated signals comparison of time-domain on Set *R1* of *PU dataset* and real signals (a)Inner ring fault (b) Outer ring fault (c) Cage fault.

Comparing the time-domain of the generated signals with real signals reveals a high degree of similarity, confirming the ability of the proposed method to generate signals under unseen working conditions that closely resemble real signals. This verifies the effectiveness and practicality of the generative model. On the frequency-spectrum comparison between the generated signals and the real signals is shown in **Figure 8**. The frequency spectrum of the generated signal and the real signal has a high degree of coincidence, especially in the low-frequency band where contains most damage features according to the vibration theory of bearing fault.

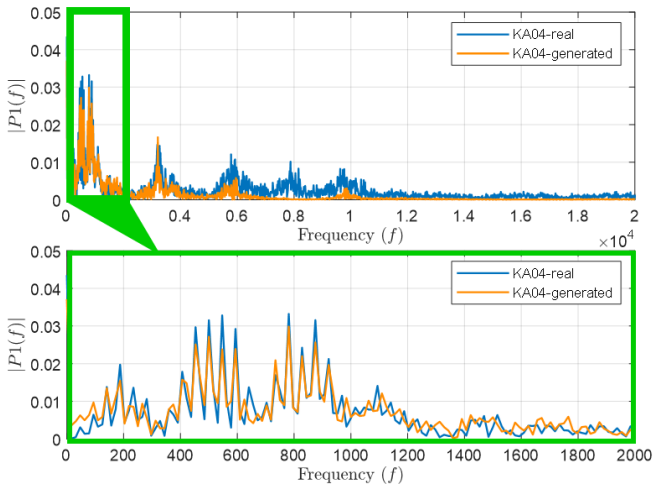

Figure 8. Generated signals comparison of frequency-domain on Set *R1* of *PU dataset* and real signals (a)Inner ring fault (b) Outer ring fault (c) Cage fault.

4.2.2. Experimental results and analysis

Table 4. presents the diagnostic results for the proposed method and comparison methods in Case 1 (SDUST dataset) and Case 2 (PU dataset). Several conclusions can be drawn. Firstly, the basic DA method achieves notably lower average test accuracies of 76.46% and 80.63% in the two cases respectively, indicating interference among data distributions during training, affecting model generalization. Secondly, DA methods using MMD, JMMD, and CORAL exhibit improvements over basic ERM, with average accuracy gains of 1.57%, 12.06%, and 10.05% respectively in Case 1, and 4.04%, 5.27%, and 3.49% in Case 2. These methods aim to eliminate distributional discrepancies between source domains and learn domain-invariant representations. Finally, the proposed method achieves the best diagnostic performance in almost all DA cases, with the highest average accuracy of 94.15% and 93.27% in both experimental cases. Furthermore, it demonstrates superior stability compared to com-parison methods in most cases. **Figure 9.** illustrates the classification accuracy of different diagnostic cases for Case 1 and Case 2, aiding in the comparison of diagnostic results.

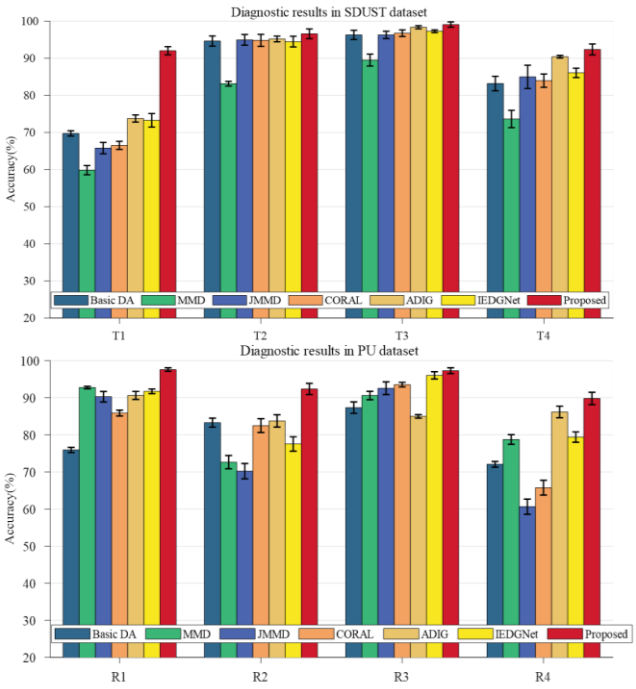

Figure 9. Classification accuracy of the different diagnostic cases of case 1 and case 2.

Table 4. Diagnostic accuracy (%) of Case 1 and Case2.

	M1	M2	M3	M4	M5	M6	Proposed
Case1							
T1	59.73±1.43	59.85±2.48	65.8±3.05	66.51±2.2	73.75±1.91	73.27±3.64	93.03±2.17
T2	84.65±2.72	83.14±1.28	94.95±2.9	94.81±3.27	95.19±1.52	94.48±2.86	95.6±2.64
T3	86.28±2.47	89.51±3.21	96.28±1.98	96.76±1.8	98.35±0.84	97.27±0.74	98.06±1.42
T4	83.19±3.89	83.62±4.67	84.98±6.26	83.96±3.6	90.42±0.76	86.06±2.49	91.37±2.94
Average	76.46±2.63	78.03±4.66	88.52±3.55	86.51±2.72	88.42±1.26	88.77±2.93	94.15±2.54
Case 2							
R1	75.92±1.38	92.75±0.69	90.26±2.87	85.86±1.59	90.61±2.17	91.73±1.26	97.6±0.92
R2	83.26±2.42	72.64±3.57	70.19±4.15	82.47±3.73	83.74±3.33	77.54±3.89	92.36±3.02
R3	87.33±3.07	90.59±2.26	92.57±3.42	93.52±1.24	84.98±0.94	96.02±1.96	97.29±1.55
R4	72.04±1.53	78.73±2.59	60.61±4.11	65.73±3.97	86.17±3.12	79.39±2.78	89.81±3.31
Average	80.63±2.10	84.67±2.27	79.41±3.64	85.89±2.63	87.38±2.39	87.17±2.47	93.27±2.21

4.2.3. Feature visualization and analysis

Compared methods based on domain adaptation (DA) aim to learn domain-invariant features, while our diagnosis seeks to generate physic-embedded signals to cover unseen distributions. we employ feature visualization to validate these conclusions. To illustrate the distribution of fault features from seen and unseen domains corresponding to seen and unseen working conditions, we present 2-D features from the second layer of the fault classifier using T-SNE (van der Maaten and Hinton 2008). For clarity, we plot the feature vectors of the SDUST dataset (Case 1) from four health conditions under case T1and four colors represent four domains, with gray points indicating features extracted from unseen domains, while other colors denote features from available source do-mains.

The domain adaptation (DA) based method aims to extract generalized features that are consistent across different domains, including unseen domains. However, as illustrated in **Figure 10**, the features learned by methods M1-M3 fail to capture the generalized representation of the I02 fault due to significant domain discrepancies between seen and unseen working conditions. Although method M4 may learn more robust features compared to M1-M3, it struggles to cluster effectively in the seen domains of I02.

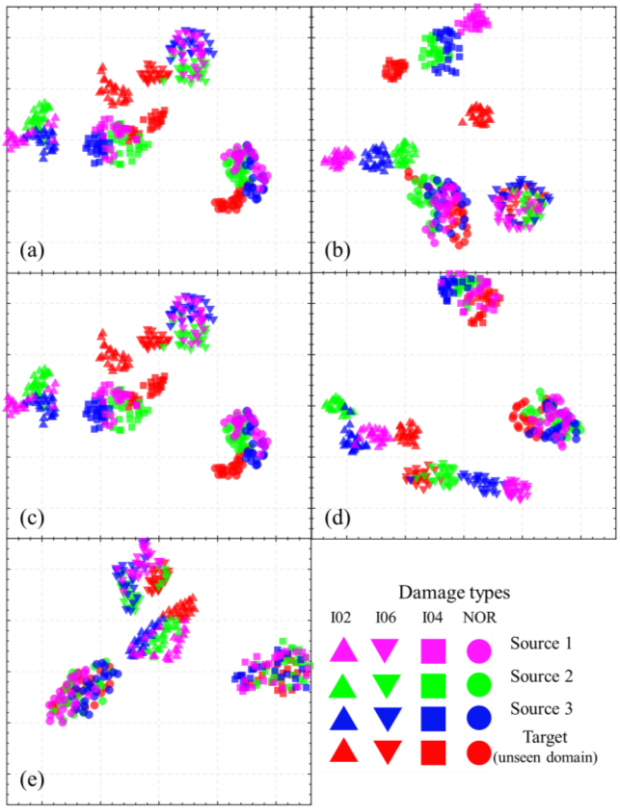

Figure 10. Results of feature-dimension reduction via T-SNE under unseen target working condition:M1, (b) M2, (c) M3, (d) M4, (e) Proposed.

In contrast, the proposed DiffPhysiNet method, leveraging the feature embedding capability of Physi-UNet, can generate signals with more domain-invariant features. This leads to improved classifier training and reaffirms that the Physi-UNet structure enables the model to fit not only the source data distribution but also data from unseen working conditions.

4.2.4. Parameter sensitivity analysis

Adjustable parameters are involved in the construction and training of the proposed method and considering their impact on the model performance, parameter sensitivity analyses are performed on all case.

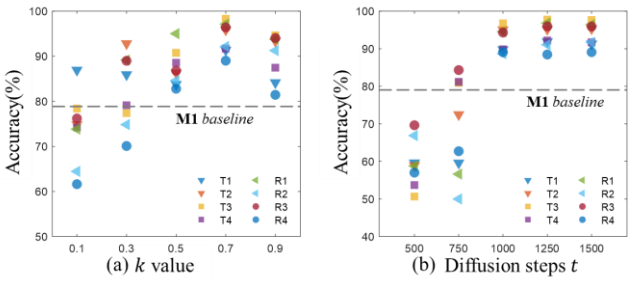

Figure 11. Parameter sensitivity analysis (a) k value: the portion of selected nearest generated samples. (b) Diffusion steps t: the iteration steps of generation progress.

k value represents the proportion of selected samples ($k = n / N$), where N is the total number of generated samples and n is the number of selected samples among them. These selected samples undergo the nearest distribution process in the K-means clustering algorithm, as depicted in **Figure 5**, where the Boundary Decision is determined by the k value. Figure **11**(a) illustrates the diagnostic accuracy for each case under different k values ranging from 0.1 to 0.9. The graph indicates that when k is below 0.5, meaning less than half of the total generated samples are selected, the performance is inferior to the baseline M1 method. This could be attributed to the reduced generation capability resulting from a smaller set of selected samples, causing offsets in the feature distribution from the real distribution. Conversely, if k is too large, the model's performance declines, likely due to the utilization of too many substandard generated signals for diagnostic model training. Hence, selecting a value of k around 0.7 is recommended.

t is the parameter of diffusion steps, the larger the value of diffusion steps the more detailed the signal generation process will be, as well as the larger the model training time and the computational resources it will consume. As shown in Figure **11** (b), it can be concluded that the performance of DiffPhysiNet framework becomes better and more stable as t is bigger than 1000 steps. Regarding the performance of M1 method as the baseline, the diffusion steps should not be less than 1000. As t increased from 1000 to 1500, the

performance of the model stabilizes and does not improve significantly.

5. CONCLUSION

In conclusion, we propose the DiffPhysiNet framework for diagnosing bearing faults under unseen working conditions for safety-critical equipment. Leveraging a generative diffusion model and working conditional encoding (WCE), this framework effectively embeds signal features, and the UCFilter method ensures signal quality using principles from K-means clustering. Experimental validation on real-world bearing datasets demonstrates the superiority of Physi-UNet over existing approaches, particularly in diagnostic accuracy. Feature visualization confirms the framework's ability to capture generalized signal features under unknown conditions, highlighting the generative model's efficacy in signal generation.

ACKNOWLEDGMENT

This work was supported by the National Natural Science Foundation of China (Grant No. 52302446) and National Natural Science Foundation of China Excellent Youth Fund (Grant No. 52322215).

REFERENCES

Ben-David, S., J. Blitzer, K. Crammer, A. Kulesza, F. Pereira, and J. W. Vaughan. 2010. 'A theory of learning from different domains', *Machine Learning*, 79: 151-75.

Benitez, Jose Antonio Lara, Takashi Furuya, Florian Faucher, Xavier Tricoche, and Maarten V. de Hoop. 2023. 'Fine-tuning Neural-Operator architectures for training and generalization', *Arxiv*.

Chen, L., Q. Li, C. Q. Shen, J. Zhu, D. Wang, and M. Xia. 2022. 'Adversarial Domain-Invariant Generalization: A Generic Domain-Regressive Framework for Bearing Fault Diagnosis Under Unseen Conditions', *Ieee Transactions on Industrial Informatics*, 18: 1790-800.

Chen, Z. Y., and W. H. Li. 2017. 'Multisensor Feature Fusion for Bearing Fault Diagnosis Using Sparse Autoencoder and Deep Belief Network', *Ieee Transactions on Instrumentation and Measurement*, 66: 1693-702.

Cui, W., J. Ding, G. Y. Meng, Z. Y. Lv, Y. H. Feng, A. M. Wang, and X. W. Wan. 2023. 'Fault Diagnosis of Rolling Bearings in Primary Mine Fans under Sample Imbalance Conditions', *Entropy*, 25.

Dang, Z. R., and M. Ishii. 2022. 'Towards stochastic modeling for two-phase flow interfacial area predictions: A physics-informed reinforcement learning approach', *International Journal of Heat and Mass Transfer*, 192.

Han, T., Y. F. Li, and M. Qian. 2021. 'A Hybrid Generalization Network for Intelligent Fault Diagnosis of Rotating Machinery Under Unseen Working Conditions', *Ieee Transactions on Instrumentation and Measurement*, 70.

Hu, C. F., Y. X. Wang, and J. W. Gu. 2020. 'Cross-domain intelligent fault classification of bearings based on tensor-aligned invariant subspace learning and two-dimensional convolutional neural networks', *Knowledge-Based Systems*, 209.

Huang, Z. L., Z. H. Lei, G. R. Wen, X. Huang, H. X. Zhou, R. Q. Yan, and X. F. Chen. 2022. 'A Multisource Dense Adaptation Adversarial Network for Fault Diagnosis of Machinery', *Ieee Transactions on Industrial Electronics*, 69: 6298-307.

Jia, S. X., J. R. Wang, B. K. Han, G. W. Zhang, X. Y. Wang, and J. T. He. 2020. 'A Novel Transfer Learning Method for Fault Diagnosis Using Maximum Classifier Discrepancy With Marginal Probability Distribution Adaptation', *Ieee Access*, 8: 71475-85.

Jiao, J. Y., M. Zhao, J. Lin, and K. X. Liang. 2020. 'Residual joint adaptation adversarial network for intelligent transfer fault diagnosis', *Mechanical Systems and Signal Processing*, 145.

Kordestani, M., M. Saif, M. E. Orchard, R. Razavi-Far, and K. Khorasani. 2021. 'Failure Prognosis and Applications-A Survey of Recent Literature', *Ieee Transactions on Reliability*, 70: 728-48.

Lehmann, F., F. Gatti, M. Bertin, and D. Clouteau. 2024. '3D elastic wave propagation with a Factorized Fourier Neural Operator (F-FNO)', *Computer Methods in Applied Mechanics and Engineering*, 420.

Li, R. R., S. M. Li, K. Xu, J. T. Lu, G. R. Teng, and J. Du. 2021. 'Deep domain adaptation with adversarial idea and coral alignment for transfer fault diagnosis of rolling bearing', *Measurement Science and Technology*, 32.

Li, W. H., R. Y. Huang, J. P. Li, Y. X. Liao, Z. Y. Chen, G. L. He, R. Q. Yan, and K. Gryllias. 2022. 'A perspective survey on deep transfer learning for fault diagnosis in industrial scenarios: Theories, applications and challenges', *Mechanical Systems and Signal Processing*, 167.

Li, X., W. Zhang, Q. Ding, and J. Q. Sun. 2020. 'Intelligent rotating machinery fault diagnosis based on deep learning using data augmentation', *Journal of Intelligent Manufacturing*, 31: 433-52.

Michau, G., and O. Fink. 2019. 'Domain Adaptation for One-Class Classification: Monitoring the Health of Critical Systems Under Limited Information', *International Journal of Prognostics and Health Management*, 10.

Rafiq, M., G. Rafiq, and G. S. Choi. 2022. 'DSFA-PINN: Deep Spectral Feature Aggregation Physics

Informed Neural Network', *Ieee Access*, 10: 22247-59.

Rombach, K., G. Michau, and O. Fink. 2023. 'Controlled generation of unseen faults for Partial and Open-Partial domain adaptation', *Reliability Engineering & System Safety*, 230.

Shu, D. L., Z. J. Li, and A. B. Farimani. 2023. 'A physics-informed diffusion model for high-fidelity flow field reconstruction', *Journal of Computational Physics*, 478.

Si, Y. N., J. X. Pu, S. F. Zang, and L. F. Sun. 2021. 'Extreme Learning Machine Based on Maximum Weighted Mean Discrepancy for Unsupervised Domain Adaptation', *Ieee Access*, 9: 2283-93.

van der Maaten, L., and G. Hinton. 2008. 'Visualizing Data using t-SNE', *Journal of Machine Learning Research*, 9: 2579-605.

Wang, K. W., X. Zhang, Q. S. Hao, Y. Wang, and Y. Shen. 2019. 'Application of improved least-square generative adversarial networks for rail crack detection by AE technique', *Neurocomputing*, 332: 236-48.

Wang, X., C. Q. Shen, M. Xia, D. Wang, J. Zhu, and Z. K. Zhu. 2020. 'Multi-scale deep intra-class transfer learning for bearing fault diagnosis', *Reliability Engineering & System Safety*, 202.

Zio, E. 2022. 'Prognostics and Health Management (PHM): Where are we and where do we (need to) go in theory and practice', *Reliability Engineering & System Safety*, 218.

Zuo, L., F. J. Xu, C. H. Zhang, T. F. Xiahou, and Y. Liu. 2022. 'A multi-layer spiking neural network-based approach to bearing fault diagnosis', *Reliability Engineering & System Safety*, 225.

BIOGRAPHIES

Zhibin Guo was born in Zhengzhou, Henan, China, in 2001. He is currently pursuing the D.E. degree in transportation engineering with Central South University, Changsha, China. His current research interests include rotating machine diagnosis, PHM for railway infrastructure, health management of highspeed train bogie, and deep learning.

Jingsong Xie was born in Anren, Hunan, China, in 1989. He received the B.S. degree from the School of Mechanical Engineering, Northwestern Polytechnical University, Xi'an, China, in 2013, and the Ph.D. degree in mechanical engineering from Xi'an Jiaotong University, Xi'an, in 2018. He joined the School of Traffic and Transportation Engineering, Central South University, Changsha, China, as a Lecturer. His research interests include fault diagnosis, machine learning, vibration analysis, and crack diagnosis.

Tongyang Pan was born in Shaanxi, China, in 1994. He received the B.S. and Ph.D. degrees in mechanical engineering from Xi'an Jiaotong University, Xi'an, China, in 2017 and 2022 respectively. He is currently a lecturer with Central South University, Changsha, China. His research interests include mechanical signal processing, intelligent fault diagnosis, and machinery condition monitoring

Tiantian Wang received the bachelor's and Ph.D. degrees from Beihang University, Beijing, China, in 2012 and 2018, respectively. He is currently a Professor with Central South University, Changsha, China, and Hunan University, Changsha. His current research interests include vehicle aerodynamics and vehicle structure, especially train/tunnel aerodynamics, and prognostics and health management (PHM) for trains.